scientific reports

Check for updates

OPEN

A density functional theory study of the molecular structure, reactivity, and spectroscopic properties of 2-(2-mercaptophenyl)-1-azaazulene tautomers and rotamers

Safinaz H. El-Demerdash[1]✉, Shimaa Abdel Halim[2], Ahmed M. El-Nahas[1] & Asmaa B. El-Meligy[1]✉

Five stable tautomer and rotamers of the 2-(2-Mercaptophenyl)-1-azaazulene (thiol, thione, R1, R2, and R3) molecules were studied using density functional theory (DFT). The geometries of the studied tautomer and rotamers were fully optimized at the B3LYP/6-31G(d,p) level. Thermodynamic calculations were performed at M06-2X/6-311G++(2d,2p) and ωB97XD/6-311G++(2d,2p) in the gas phase and ethanol solution conditions modeled by the solvation model based on density (SMD). The kinetic constant of tautomer and rotamers conversion was calculated in the temperature range 270–320 K using variational transition state theory (VTST) accompanied by one-dimensional wigner tunneling correction. Energy refinement at CCSD(T)/6–311++G(2d,2p) in the gas phase has been calculated. All the studied DFT methods qualitatively give similar tautomer stability orders in the gas phase. The ethanol solvent causes some reordering of the relative stability of 2-(2-Mercaptophenyl)-1-azaazulene conformers. The transition states for the 2-(2-Mercaptophenyl)-1-azaazulene tautomerization and rotamerization processes were also determined. The reactivity, electric dipole moment, and spectroscopic properties of the studied tautomer and rotamers were computed. The hyper-Rayleigh scattering (β_{HRS}), and depolarization ratio (DR) exhibited promising optical properties when nonlinear optical properties were calculated.

Tautomerism provides knowledge of the variety of forms in which organic molecules can exist. Many biologically active compounds, including pyrazolone derivatives, take part in tautomeric transformation[1]. In numerous fields of chemistry, intramolecular proton transfer (IPT) is crucial[2]. Its mechanism takes place in both ground and excited states[3]. Compounds that exhibit intramolecular proton transfer can be used as laser dyes, fluorescent probes, high-energy radiation detectors, memory storage devices, and polymer protectors[4]. Hence, molecules that have intramolecular proton transfer have received great interest from an experimental and theoretical perspective[5,6]. Numerous topics in organic chemistry and biochemistry can be studied more effectively by understanding the nature of tautomeric equilibrium[7].

Thione–thiol tautomerization is a remarkable subject that has attracted a lot of study. The thione tautomer is mostly detected in the gas phase under standard experimental conditions. Thiol tautomers of thione compounds, which can be stabilized in inert matrices at lower temperatures, can be subjected to UV light. These compounds include (1H)-pyridinethione[8], 4(3H)-pyrimidinethione and 3(2H)-pyridazinethione[9], 2(1H)-quinolinethione[10], methimazole[11], 2-thiobenzimidazole[12], thiourea[13], and thioacetamide[14]. Thiophenol is a notable exception that only exists as a thiol tautomer[15]. Organosulfur compounds containing thiocarbonyl groups have attracted interest because of their diverse chemistry[16], various biological applications[17,18], and the ability of the C = S bond to oxidize quickly to form the corresponding thiols and disulfides[19].

[1]Chemistry Department, Faculty of Science, Menoufia University, Shebin El-Kom 32512, Egypt. [2]Chemistry Department, Faculty of Education, Ain Shams University, Cairo, Egypt. ✉email: hamdysafinaz@yahoo.com; asmaaphys@yahoo.com

Azaazulenes have attracted a lot of attention because of their chemical, physical, and biological activities[20]. Azaazulene is an aromatic heterocyclic compound. It stands for a significant class of compounds with systems of π- and n-electrons. Oda et al.[21] investigated 2-(2-Hydroxyphenyl)-1-azaazulene's production, molecular structure, and characteristics. In addition, the structures, energetics, and spectra of 2-(2-Hydroxyphenyl)-1-azaazulene tautomers have been examined using B3LYP, M06-2X, B97XD, and CCSD(T) with various basis sets[22]. The biological potential of its counterpart, 2-(2-Mercaptophenyl)-1-azaazulene, is anticipated. In order to fully understand the researched compound's expected distinctive biological properties, its electronic structure must also be investigated, along with its electronic and optical spectra. The 2-(2-Mercaptophenyl)-1-azaazulene structure is classified as an organic semiconductor of a small molecule and is designed as a π-conjugated nanostructure. It also has a significant extinction coefficient, good light gain, and a delocalization of electrons. These materials are suitable for optoelectronic devices as a result of their highly appealing electrical and optical properties[23]. There haven't been any theoretical or experimental studies on 2-(2-Mercaptophenyl)-1-azaazulene. So, we will study the thiol-thione tautomerization of 2-(2-Mercaptophenyl)-1-azaazulene (Fig. 1) in the gas phase and ethanol.

The standard methods for studying tautomeric transformations in solutions and in the crystalline state include X-ray crystallography, nuclear magnetic resonance spectrometry, ultraviolet radiation, infrared spectrophotometry, and quantum chemistry[24,25]. Using DFT and TD-DFT, quantum-chemical calculations can estimate minimal computational needs and provide excellent findings from experiments[26,27]. As a result, they are particularly interesting for researching tautomeric compounds[26,27]. However, the results always remain confined to the level of the theory and basis sets that were employed[28,29].

In the current study, we use the B3LYP functional in the DFT approach to study 2-(2-Mercaptophenyl)-1-azaazulene's molecular structure, thermodynamic and kinetic stabilities for the first time. Additionally, equilibrium constants, reactivity, and spectroscopic properties of the different tautomeric structures of 2-(2-Mercaptophenyl)-1-azaazulene will be studied using different quantum chemical methods. The electrical and optical properties of these tautomers are also shown by NLO analysis, which also explains charge transport inside them.

Computational details

The commonly used B3LYP method has provided the correct molecular geometries, activation energies, and energy differences between pairs of tautomers, similar to MP2-level predictions[30]. It has been concluded that the small absolute errors and the cost-effectiveness of the computations make the B3LYP method a good choice for these systems[30]. Our computations were carried out using the gradient-corrected hybrid density functional B3LYP DFT method[31]. For each structure, a full geometry optimization without symmetry constraints was performed using this functional along with the 6-31G(d,p) basis set[32] as implemented by the Gaussian 09 package[33]. All geometries were visualized either using GaussView 5.0.9[34] or ChemCraft 1.6[35] programs.

The presence of one imaginary frequency that the ChemCraft program evaluated corroborated the presence of TSs[35]. Real frequencies are shown by Minima. Using the 6–311++G(2d,2p) basis set at the B3LYP/6-31G(d,p) optimized structures, energies were adjusted at the meta-hybrid generalized gradient approximation (M06-2X)[36,37] and long-range corrected hybrid functional of Becke's 97 that incorporates dispersion correction (ωB97XD)[38,39] functionals. The CCSD(T)[40] computations are a potent tool for precise estimation of reaction and activation energies for species when a single-reference wavefunction is a good approximation. As a result, we used the

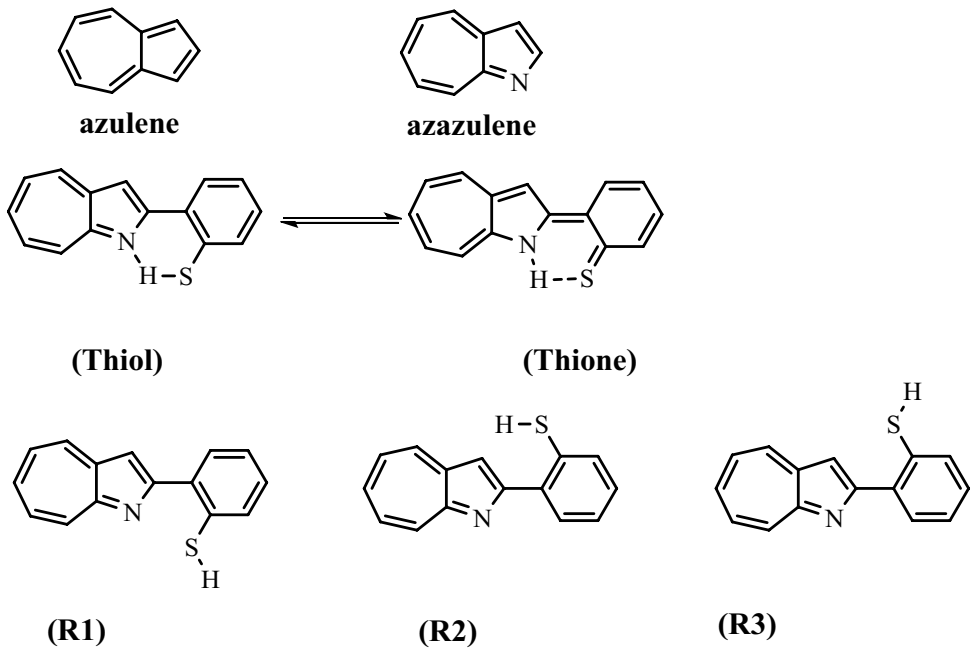

Figure 1. The tautomeric and rotameric structures of 2-(2-Mercaptophenyl)-1-azaazulene.

B3LYP/6–31+G(d,p) geometries to do single point energy calculations at CCSD(T)/6–311 ++G(2d,2p). The findings show that, in comparison to the more precise (CCSD(T)/6–311++G(2d,2p) level, ωB97XD/6–311++G(2d,2p) performs marginally better than M06-2X/6–311++G(2d,2p). Therefore, for discussion of energetics, the level ωB97XD/6–311+ +G(2d,2p) is used unless otherwise stated.

The solvation effect has been modeled in ethanol using the solvation model based on density (SMD)[41] at the B3LYP/6–31+G(d,p) level for all the tautomers and rotamers. We estimated solvation energies in ethanol as single point energy calculations on geometries optimized in ethanol at B3LYP using M06-2X, B3LYP, and ωB97XD functionals with 6–311++G(2d,2p) basis sets.

On the basis of the statistical thermodynamics principle[42], the entropy (*S*) and enthalpy (*H*) of the tautomers in all environments at standard conditions of $T = 298.15$ K and $P = 1$ atm have been obtained. Gibbs free energy values, which were calculated at the same levels of theory, were used for the evaluation of the tautomeric equilibrium constants. For the tautomerization and rotamerization transformation processes, rate coefficients were calculated in the temperature range 270–320 K (k_{uni}, in s^{-1}) using the variational transition state theory (CVT)[43] that includes generalized transition state rates k^{GT} with wigner tunneling correction ($\chi(T)$)[44] according to (1–3) equations.

$$k^{GT}(T) = \sigma \frac{K_b T}{h} \frac{Q^{TS}(T,s)}{N_A Q^R(T)} e^{-V^{\#}(S)/K_b T} \tag{1}$$

$$k^{CVT}(T) = \min K^{GT}(T,s) \tag{2}$$

$$\chi(T) = 1 + \frac{1}{24}\left(\frac{h\nu}{K_b T}\right)^2 \tag{3}$$

where σ, k_b, T, h, R, and s refer to the reaction path degeneracy, Boltzmann constant, temperature in Kelvin, Planck constant, ideal gas constant, and the distance along the minimum energy reaction path (MEP) in isoinertial coordinates, respectively.

Global chemical reactivity descriptors[45] have been calculated using the energies of the highest occupied and lowest unoccupied molecular orbitals (HOMO and LUMO), respectively, to better comprehend the reactivity and stability of the structures under study. Accordingly, for B3LYP/6-31G(d,p) in the gas phase, the ionization potential (IP), electron affinity (EA), absolute hardness (η), softness (S), and electronegativity (χ) were calculated. The following formulas have been used to calculate the global chemical reactivity descriptors:

$$\mathrm{IP} = -\mathrm{E_{HOMO}} \tag{4}$$

$$\mathrm{EA} = -\mathrm{E_{LUMO}} \tag{5}$$

$$\eta = (\mathrm{E_{LUMO}} - \mathrm{E_{HOMO}})/2 \tag{6}$$

$$\mathrm{S} = 1/2\eta \tag{7}$$

$$\chi = -(\mathrm{E_{LIUMO}} + \mathrm{E_{HOMO}})/2 \tag{8}$$

Nucleus-independent chemical shift (NICS) computations have been performed for each compound in the gas phase at the same level of optimization (B3LYP/6-31G(d,p)). Particularly, the computed NICS values are NICS(0)iso, which refers to the absolute isotropic shielding at the center of the ring; NICS(0)zz, which is the total contribution to the orthogonal to the plane component of the NICS tensor, assuming the molecule lies in the xy-plane; as well as NICS(1)iso and NICS(1)zz, which are analogue indices computed at 1 A above the center of the ring[46,47]. The geometry-based index harmonic oscillator measure of aromaticity (HOMA)[48,49], which makes use of bond lengths in accordance with Krygowski's[48] instructions, is another criterion of aromaticity. Electrostatic potential (ESP) surfaces have been derived from the B3LYP/6–31G(d,p) calculation.

UV–vis spectra for the investigated structures were computed at TD-DFT PBE[50,51] (TD-PBE/6–311+G(d,p)) using the SMD method at the B3LYP/6-31G(d,p) optimized gas-phase geometry in acetonitrile. The electron excitations of 2OHPhAZ were precisely determined by the Perdew-Burke-Ernzerhof technique (PBE)[22]. Gauss-Sum program[52] was used to simulate the ultraviolet–visible (UV–vis) spectra. Instead of focusing on the canonical orbitals, natural transition orbitals (NTOs)[53] were estimated for each electron excitation. We create the frontier orbitals and NTOs using Chemcraft. Additionally, we use the optimized gas-phase geometry to calculate the NMR spectra of the various tautomers and rotamers relative to the 13C and 1H isotropic chemical shielding of tetramethylsilane (TMS) at the B3LYP/6-31G(d,p) in chloroform using the gauge-independent atomic orbital (GIAO) method[54,55].

We concentrated on the hyper-Rayleigh scattering (β_{HRS}) and depolarization ratio (DR) among second-order NLO characteristics[56], and the complete equations for calculating the magnitude of the total dipole moment μ_{tot}, the average polarizability α_{tot} and the first hyperpolarizability β_{tot}, using the *x*, *y* and *z* components are as follows:[57,58]

$$\mu = \left(\mu_x^2 + \mu_y^2 + \mu_z^2\right)^{1/2} \tag{9}$$

$$\langle \alpha \rangle = 1/3(\alpha_{xx} + \alpha_{yy} + \alpha_{zz}) \tag{10}$$

$$\begin{aligned} \Delta\alpha &= \left(\left(\alpha_{xx} - \alpha_{yy}\right)^2 + \left(\alpha_{yy} - \alpha_{zz}\right)^2 + \left(\alpha_{zz} - \alpha_{xx}\right)^2/2 \right)^{1/2} \langle \beta \rangle_{tot} \\ &= \left[\left(\beta_{xxx} + \beta_{xyy} + \beta_{xzz}\right)^2 + \left(\beta_{yyy} + \beta_{xxy} + \beta_{yzz}\right)^2 + \left(\beta_{zzz} + \beta_{xxz} + \beta_{yyz}\right)^2 \right]^{1/2} \end{aligned} \tag{11}$$

$$\beta(_{HRs}) = \sqrt{\beta^2 zzz + \beta^2 zxx} \tag{12}$$

$$\mathrm{DR} = \frac{\beta^2 zzz}{\beta^2 zxx} \tag{13}$$

Results and discussion

Geometries optimization. According to previous research, the M06-2X and B97XD functionals are extremely accurate in predicting the stability of tautomers and rotamers trend[59–61]. The same order of stability was also created by B3LYP/6–31+G(d,p) as obtained by the ab initio multi-level CBS-QB3 approach[62]. Consequently, the structures will be discussed at B3LYP/6-31G(d,p), and energies will be discussed at M06-2X/6–311++G(2d,2p), B97XD/6–311++G(2d,2p), and CCSD(T)/6–311++G(2d,2p).

2-(2-Mercaptophenyl)-1-azaazulene could exist as thione-thiol tautomerism based on the movement of hydrogen atom among nitrogen and sulfur, and three rotamers form R1, R2, and R3. The optimized geometries of the studied tautomeric and rotameric forms and their corresponding inter-conversion transition states are shown in Fig. 2, and their geometrical parameters are listed in Table 1 at the B3LYP/6-31G(d,p) level. Also, Table S1 in the supplementary information (SI) reported their coordinates. The rotamer R1 is formed by rotating the OH group of thiol, while R2 and R3 are formed by rotating the phenyl ring of thiol and R1, respectively. To the best of our knowledge, there are no theoretical and experimental reports on the geometry of the titled compound conformers in the literature for comparison. The calculated geometrical parameters are in good agreement with the corresponding values reported for a similar compound[22].

The thione form in the gas phase shows that it is almost planar with a dihedral angle (N1C2C1'C2') of 0.0º, but in the case of the thiol form, the terminal phenyl ring is out of plane with a dihedral angle (N1C2C1'C2') of—13.9°. The thione-thiol tautomerization occurs via an IPT reaction. The intramolecular hydrogen bond generates a six-membered ring in both the thiol and thione tautomers. The intramolecular H-bonding is between the S1-H1' donor and N1 acceptor (1.808 Å) of the thiol tautomer, but in the case of the thione tautomer, the interaction is between the N–H donor and the thiophenol S1 acceptor, where the hydrogen-bond lengths are about 2.015 Å. In the IPT, the C2′-S1 bond length decreases from 1.779 in the thiol form to 1.735 Å in the thione form. Also, the calculated S-H1'…N hydrogen-bond angles decrease from 143.3° in the thiol form to 142.2° in the thione form.

The thiol-thione tautomer passes through the transition state (TST) (see Fig. 2). The extracted observations of the proton shift process include: (1) The S1′-H1′ bond length of 0.968 Å in thiol elongated by 0.203 Å in the TST and eventually separated to release proton; (2) The proton then migrated and approached N1 with a distance of 1.329 Å in the TST before the formation of the N1-H1' bond (1.056 Å) in thione; (3) In concerted processes, the thiol S1C2'C1' and N1 C2 C1' angles closed up by 6.2° and 1.7°, respectively, in the TST and finally settling at 126.5◦ and 122.7◦, respectively, in thione.

In the process of rotamerization, the observed slightly increased C2'-S1 bond distance for R2 and R3 (1.794 Å) compared to R1 (1.789 Å) is due to the decrease in double bond character in R2 and R3 because there is no conjugation of the sigma lone pair in R2 and R3. Additionally, there is no hydrogen bond in the R1 rotamer, and the donor–acceptor distance of 2.773 Å is smaller than the corresponding distance in thiol of 3.021 Å. The S1 – H1' bond length in TSR1 and R1 is similar but shorter than that in thiol by 0.02 Å due to the presence of HB in the latter structure. The H1' – S1 – C2' angle is rotated by 3.4° from R1. The donor–acceptor distance in TSR1 is elongated to 3.249 Å. The calculated dihedral angles show that the planarity of rotamers is distorted (Table 1). The non-rigid structure of 2-(2-Mercaptophenyl)-1-azaazulene tautomers and rotamers gives them the ability to fit with receptors in biological systems.

Tautomerism and thermodynamic properties. This section deals with the study of equilibrium between the studied tautomers and rotamers using the DFT/M06-2X and ωB97XD in comparison to the more accurate CCSD (T) calculations. Table 2 presents the theoretically computed corrected relative energies (ΔE), Gibbs free energies (ΔG), and enthalpies (ΔH) of the five tautomers and rotamers at the ωB97XD/6–311++G(2d,2p), M06-2X/6–311++G(2d,2p), and CCSD(T)/6–311++G(2d,2p) levels in the gas and ethanol phases. For tautomerization, it is found that the thiol form is more stable than the thione form in the gas phase. The relative energy difference between the thiol and thione in the gas phase is 3.30 and 5.30 kcal/mol at ωB97XD and CCSD(T), respectively. The thiol stability in the gas phase is expected by having a lower and stronger IHB than thione and by having the higher aromaticity of the phenyl ring that has been broken by the formation of the thione form (as will be discussed in Section "Aromaticity").

In the rotamerization process, the order of stability of the rotameric structures is R2 > R3 > R1. Rotamer R2 is slightly more stable than R3 and R1 by about 0.42 and 0.44 kcal/mol at ωB97XD/6–311++G(2d,2p), respectively. R1 is the least stable rotamer at all calculated levels. The stability of R2 and R3 can be attributed to the possible

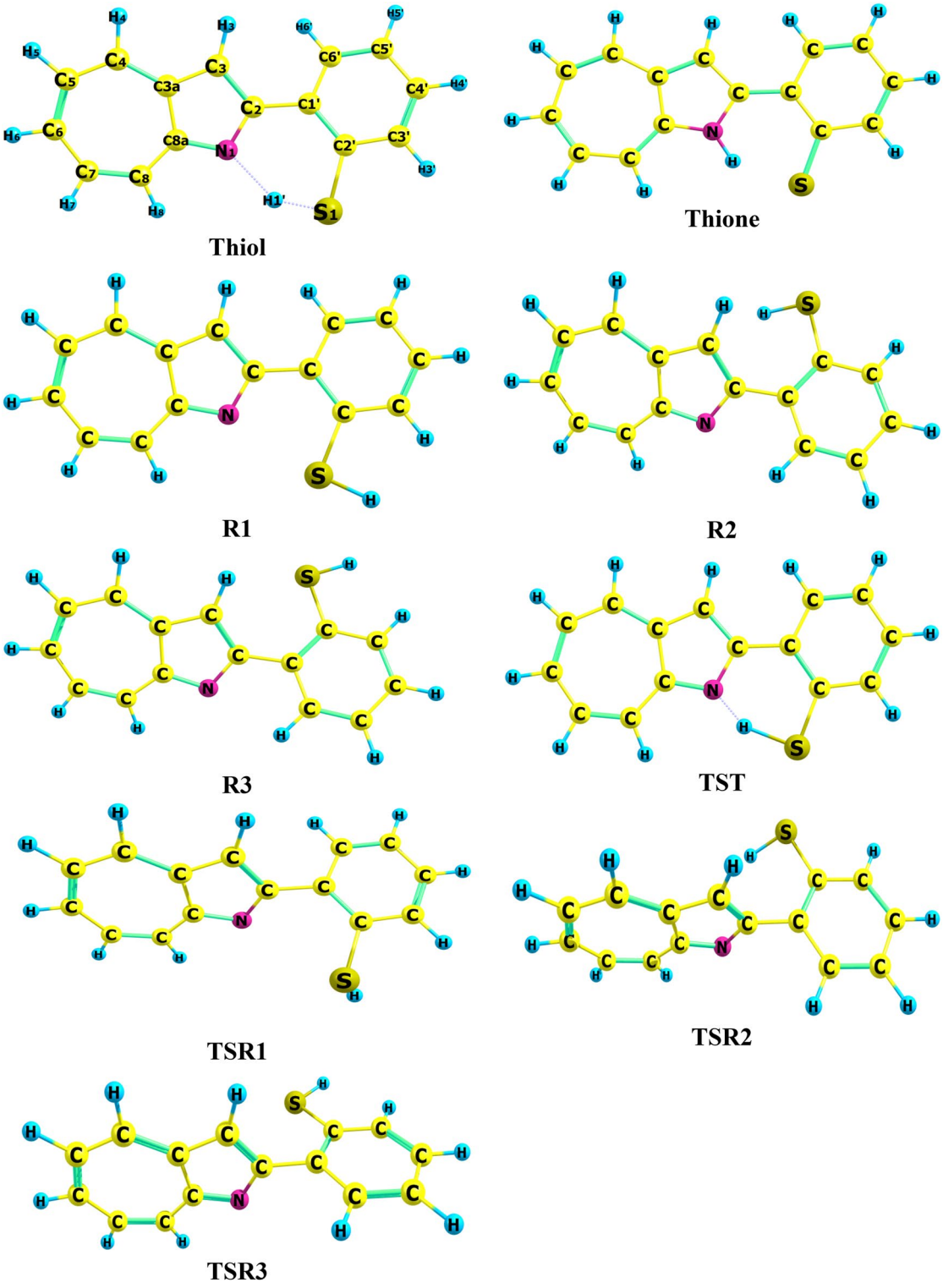

Figure 2. Optimized structures of the 2-(2-Mercaptophenyl)-1-azaazulene tautomer and rotamers with their corresponding transition states at B3LYP/6-31G d,p) in the gas phase.

intramolecular H bonding interaction of the C6′–H6′…N1 as shown in Fig. 1. The slightly higher stability of R3 than R2 can be due to the anti-position present between the S1-H1' group and the nitrogen of the azaazulene ring, given the possibility of H3 interaction with the sulfur atom.

Mezey et al.[63,64] proposed that any species with a higher energy than 10 kcal mol^{-1} above the most stable form would not exist in any appreciable concentration. So, we can conclude that all the studied tautomers and rotamers of 2-(2-Mercaptophenyl)-1-azaazulene can be observed and exist experimentally by having a low difference in

Bond/angles [a]	Thiol	Thione	R1	R2	R3
S1-H1'	1.371	2.015	1.355	1.347	1.347
N1-H1'	1.808	1.056	4.114	3.851	5.690
C2'-S1	1.779	1.735	1.790	1.794	1.794
N1-C2	1.364	1.375	1.357	1.365	1.366
C1'–C2'	1.424	1.449	1.420	1.415	1.416
C2–C1'	1.470	1.433	1.465	1.475	1.473
C2'–C3'	1.407	1.428	1.406	1.402	1.403
C8a–N1	1.349	1.359	1.348	1.346	1.344
N1H1'S1	143.3	142.2	6.7	115.2	25.2
H1'S1C2'	94.4	87.5	93.3	97.6	95.4
N1C2C1'	122.9	122.7	120.7	118.7	118.6
S1C2'C1'	126.1	126.5	122.4	125.5	121.3
S1C2'C3'	114.9	117.3	118.9	114.7	119.1
N1C2C1'C2'	−13.9	0.0	13.1	151.5	156.2
C2C1'C2'S1	0.6	0.0	0.4	−3.5	− 3.8
C1'C2'S1H1'	7.4	0.0	171.6	−25.6	− 175.1
H1'N1C2C1'	13.5	0.0	− 13.7	− 103.5	− 58.8

Table 1. Calculated bond lengths (Å) and angles (in °) of 2-(2-Mercaptophenyl)-1-azaazulene tautomers and rotamers at the B3LYP/6-31G(d,p) in the gas phase. [a]Atom numbering is given in Fig. 2.

Parameters	Thiol	Thione	R1	R2	R3	TS_T	TS_{R1}	TS_{R2}	TS_{R3}
M06-2X[a] (Gas phase)									
ΔE^0	0.00	2.89	0.94	0.68	0.77	2.10	4.38	2.53	3.57
ΔG_{298}	0.00	3.34	0.73	0.69	0.69	2.65	4.37	3.11	4.16
ΔH_{298}	0.00	2.76	1.02	0.87	0.97	1.82	4.33	2.37	3.42
μ	4.67	8.71	2.53	3.13	1.91	6.93	2.62	3.67	1.91
ωB97XD[a] (Gas phase)									
ΔE^0	0.00	3.30	1.90	1.46	1.88	2.47	4.75	2.41	3.58
ΔG_{298}	0.00	3.75	1.69	1.47	1.80	3.02	4.75	2.99	4.16
ΔH_{298}	0.00	3.16	1.98	1.65	2.08	2.19	4.70	2.25	3.42
μ	4.83	9.03	2.66	3.28	1.99	7.10	2.72	3.79	2.65
CCSD(T)[a] (Gas phase)									
ΔE^0	0.00	5.30	1.43	0.76	1.05	3.63	3.71	1.55	2.68
ΔG_{298}	0.0	5.71	0.94	0.77	0.98	4.18	3.71	2.13	3.26
ΔH_{298}	0.00	5.12	1.22	0.95	1.26	3.35	3.67	1.39	2.52
μ	5.01	10.14	2.09	3.48	2.09	7.56	2.93	3.99	2.79
M06-2X[a] (Ethanol)									
ΔE^0	4.34	0.00	4.27	4.90	4.25	4.12	7.58	5.63	5.80
ΔG_{298}	5.41	0.00	5.57	6.01	5.30	5.65	8.67	7.08	7.55
ΔH_{298}	4.36	0.00	3.80	5.15	4.52	3.83	7.58	5.58	5.66
μ	7.77	16.00	4.31	5.54	3.61	9.70	4.63	6.36	4.26
ωB97XD[a] (Ethanol)									
ΔE^0	4.50	0.00	5.42	5.49	5.30	4.39	7.93	5.40	5.87
ΔG_{298}	5,57	0.00	6.71	6.61	6.34	5.92	9.02	6.86	7.62
ΔH_{298}	4.53	0.00	4.94	5.74	5.56	5.00	7.93	5.36	5.74
μ	7.97	16.31	4.49	5.76	3.76	9.89	4.79	6.55	4.40

Table 2. Relative zero-point corrected energies (ΔE^0), relative Gibbs free energies (ΔG_{298}), enthalpies (ΔH_{298}) in kcal/mol, and dipole moments (μ; in Debye) for the 2-(2-Mercaptophenyl)-1-azaazulene tautomers, rotamers, and their transition states in the gas phase and ethanol. [a]Method/6–311++G(2d,2p)//B3LYP/6-31G(d,p).

the relative energies (Table 2). A chemical equilibrium between tautomers and rotamers is characterized by the equilibrium constant (K) that can be calculated using:

$$K = e^{-(\Delta G/RT)} \quad (14)$$

where the gas constant (R) is $1.987^{*}10^{-3}$ kcal/mol and the temperature (T) is 298.15 K and the ΔG is the difference between the Gibbs free energies of a given tautomer or rotamer relative to thiol. Table 3 collects the K values for the four possible equilibrium reactions in the gas phase and ethanol at ωB97XD/6–311++G(2d,2p) and CCSD(T)/6–311++G(2d,2p).

In accordance with the highest stability of thiol among the other tautomers and rotamers in the gas phase, K_1 has the lowest values. This implies the presence of thiol alone in the gas phase. The values of K_2, K_3 and K_4 (see Table 3) indicate that the equilibrium is effective and the rotamers with the thiol are present in comparable quantities in both the gas phase and ethanol. The calculated rate constant for the studied transformation with VTST and wigner tunneling is given in Table 4. The results show that the tautomerization transformation has a higher rate and a higher tunneling correction effect than rotamerization in the gas phase during the applied temperature range. The rate of rotamerization seems to slightly increase as the temperature is raised.

The heterocyclic tautomerism is very sensitive to the solvent nature. Therefore, more efforts have been made to study the effect of solvents such as ethanol on the stability of the tautomers and rotamers using the same levels of theory. Energy results obtained from these calculations are collected in Table 2. In contrast to the gas phase, the higher stability of the thione form than thiol in ethanol has been observed at all levels of calculations. The stability order is reversed in ethanol, and the thione becomes more stable relative to thiol by 4.50 kcal/mol at the ωB97XD/6–311++G(2d,2p) level (Table 2). Also, the higher value of the equilibrium constant ($1.208^{*}10^{4}$) emphasized the higher stability of thione in the ethanol solvent (Table 3).

From both theoretical and experimental points of view, the thione-thiol tautomer reaction presents challenges. Computational studies of sulfur-containing molecules often show large basis set effects[65,66]. There is evidence that the thione-thiol tautomeric equilibrium between 2-pyridinethiol (2SH) and 2-pyridinethione (2S) also strongly depends on the environment. 2S is generally believed to be more stable in polar solvents[67,68] while 2SH has high stability in the gas phase and non-polar solvents[69,70]. The stability order of thione-thiol tautomers of 2-(2-Mercaptophenyl)-1-azaazulene agrees with the predominance of 2-pyridinethione (thione form) over 2-pyridinethiol (thiol form) in polar solvents[67,68].

The calculated dipole moment values for all tautomers and rotamers at the ωB97XD/6–311++G(2d,2p) level of theory in the gas and ethanol phases are given in Table 2. It can be noted that thione has the highest polarity. As a result, it has a significant impact on the stability order in ethanol as a polar solvent. Obviously, a larger dipole moment leads to greater stabilization. As can be seen in Table 2, the thione has 16.31 D, while the thiol, R1, R2 and R3 have 7.97, 4.49, 5.76 and 3.76 D, respectively, at ωB97XD/6–311++G(2d,2p) level of theory in the ethanol phase.

Equilibrium reaction		ωB97XD[a]		CCSD(T)[a]
		Gas phase	Ethanol	Gas phase
Thiol $\overset{k1}{\leftrightarrow}$ thione	K_1	0.002	1.208×10^{4}	6.551×10^{-5}
Thiol $\overset{k2}{\leftrightarrow}$ R1	K_2	0. 058	0.146	0.206
Thiol $\overset{k3}{\leftrightarrow}$ R2	K_3	0.084	0.172	0.272
Thiol $\overset{k4}{\leftrightarrow}$ R3	K_4	0.048	0.270	0.193

Table 3. Equilibrium constants for 2-(2-Mercaptophenyl)-1-azaazulene tautomers and rotamers in gas phase and ethanol at ωB97XD[a]/6–311++G(d,p) basis set and CCSD(T)/6–311++G(d,p). [a]Method/6–311++G2d,2p)//B3LYP/6-31G(d,p).

	Thiol → thione (TS_T)		Thiol → R1 (TS_{R1})		Thiol → R2 (TS_{R2})		Thiol → R3 (TS_{R3})	
T (K)	$\chi(T)$	k^{CVT}	$\chi(T)$	k^{CVT}	$\chi(T)$	k^{CVT}	$\chi(T)$	k^{CVT}
270	2.23	1.64E + 12	1.06	4.72E + 06	1	1.66E + 07	1	3.78E + 06
280	2.14	1.67E + 12	1.05	8.05E + 06	1	2.60E + 07	1	6.23E + 06
290	2.06	1.71E + 12	1.05	1.32E + 07	1	3.95E + 07	1	9.94E + 06
300	1.99	1.74E + 12	1.05	2.11E + 07	1	5.84E + 07	1	1.54E + 07
310	1.93	1.77E + 12	1.04	3.26E + 07	1	8.42E + 07	1	2.31E + 07
320	1.87	1.80E + 12	1.04	4.90E + 07	1	1.19E + 08	1	3.40E + 07

Table 4. Lists the VTST rate constant and wigner tunneling of the tautomerization and rotamerization conversion processes over a temperature range 270–320 K at B3LYP/6-31G(d,p) in the gas phase.

Comparing the previous findings with those of the ethanol phase, it is observed that the relative energy difference is positive for all the tautomers and rotamers. This result suggests that the presence of ethanol helps stabilize them, with a clear stabilization of five tautomers and rotamers. For the given tautomers and rotamers, the results show that the thiol form has the lowest formation enthalpy values (Table 2) in the gas phase. This means that it is more stable than the thione form. The lower positive reaction enthalpies mean that the equilibrium reaction is an endothermic one.

Chemical reactivity. *Theory of frontier molecular orbitals.* HOMO and LUMO orbitals play a fundamental role in the qualitative interpretation of chemical reactivity[71]. The energy gap between HOMO and LUMO frontier orbitals is one of the significant characteristics of molecules and plays an important role in electric properties, electronic spectra, and photochemical reactions. The HOMO–LUMO energy gap helps characterize the chemical reactivity and kinetic stability of the molecule[72]. A molecule with a high energy gap (ΔE) is less polarizable and is generally associated with low chemical reactivity and high kinetic stability[73]. Table 5 contains the energies of the HOMO LUMO boundary orbitals and the HOMO–LUMO energy gaps in gas and ethanol phases. The energy gap values decrease in the ethanol (Table 5) compared with those obtained in the gas phase. Therefore, the tautomers and rotamers are more reactive in ethanol. The obtained value of the thione tautomer ($\Delta E_{gap} = 1.87$ and 0.08 eV) is smaller than those obtained with thiol ($\Delta E_{gap} = 2.98$ and 0.12 eV) in gas and ethanol, respectively. So, thione is the most polarizable and has the highest interactions for intramolecular charge transfer. The large energy gap of the thiol confirms the high stability of the thiol tautomer. The rotamers (R1-R3) are hard molecules and have the least ability to polarize because they have a higher energy gap than tautomers. R3 has the largest value of the energy gap, 3.44 and 0.13 eV in the gas phase and ethanol, respectively.

Global indices of reactivity. The study of the global reactivity of molecules is based on the calculation of global indices deduced from electronic properties. The global indices of the reactivity in the gas phase and ethanol of the studied conformers are recorded in Table 5. Chemical hardness (η) and global softness (S) express the resistance of a system to a change in its number of electrons. In a given series of molecules, when η is weak, the molecule is called soft and when it is high, the molecule is called hard. This is quite the opposite of softness, which evolves in the opposite direction of hardness[74]. The value of the chemical hardness of thione is the lowest, where $\eta = 0.93$ and 0.04 eV in the gas phase and ethanol, respectively. Also, we note that the thione form has a lower electronegativity value ($\chi = 3.77$ eV) than other tautomers and rotamers in the gas phase, which supports the stability of thiol in the gas phase.

Electrostatic potential (ESP). The electrostatic potential (ESP) surface is another useful tool to understand the chemical reactivity of a molecule. The ESP study shows that H-donor and H-acceptor properties of molecules are revealed by positive and negative regions, respectively[75].

By using ESP maps, the charged areas of the molecule can be shown. In ESP maps, the regions with the highest negative electrostatic potential are shown in red, while those with the most positive electrostatic potential are shown in blue. Figure 3 shows the ESP surfaces of the examined structures derived using the B3LYP/6-31G (d,p). The ESP of thiol, thione, and R1 shows that a substantial amount of negative charge is localized on the S atom, with just a tiny amount of negative charge localized on the sulfur atom for R1.

As a result, the S atom is believed to have the highest electron donation ability towards the formation of a H-bond or metal ions. The blue colour around the H atoms indicates their positive charge. For R2 and R3 the negativity charge becomes localized on the N atom. Therefore, R2 and R3 have a high tendency to bind with metal ions on the N side.

	E_{HOMO}	E_{LUMO}	E_g	*IP*	*EA*	*X*	η	*S*
Tautomers/rotamers (Gas phase)								
Thiol	−5.42	−2.44	2.98	5.42	2.44	3.93	1.49	0.75
Thione	−4.70	−2.83	1.87	4.70	2.83	3.77	0.93	0.47
R1	−5.49	−2.25	3.24	5.49	2.25	3.87	1.62	0.81
R2	−5.70	−2.33	3.37	5.70	2.33	4.01	1.68	0.84
R3	−5.67	−2.23	3.44	5.67	2.23	3.95	1.72	0.86
(Ethanol phase)								
Thiol	−0.204	−0.084	0.129	0.204	0.085	0.144	0.06	0.03
Thione	−0.178	−0.094	0.084	0.178	0.095	0.137	0.04	0.02
R1	−0.207	−0.081	0.125	0.207	0.081	0.144	0.06	0.03
R2	−0.211	−0.082	0.129	0.211	0.082	0.146	0.06	0.03
R3	−0.212	−0.081	0.130	0.211	0.081	0.146	0.07	0.03

Table 5. Global chemical descriptor (eV) of the studied structures at B3LYP/6-31G (d,p) in the gas phase and ethanol.

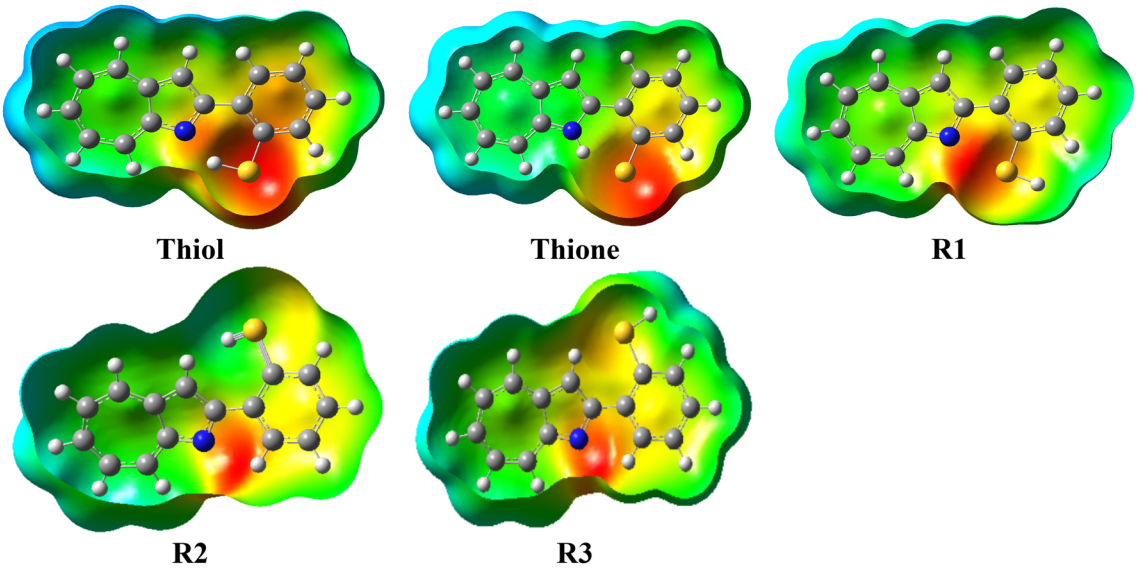

Figure 3. Molecular ESP surfaces of the investigated structures at the B3LYP/6-31G(d,p) in gas phase.

Aromaticity. The aromaticity of organic compounds is one of the most important characteristics related to their specific chemical reactive structure[76]. In this study, we used some aromaticity indicators that depend on geometry. HOMA is one of the best ways to describe the change in aromaticity[48,49]. When HOMA is unity[66], then the compound is completely aromatic, while if HOMA equals zero (0), the compound or ring is completely non-aromatic. More aromatic rings have more π-electrons delocalized, and this is indicated by rings with higher HOMA values. HOMA can be calculated according to the following equation:

$$HOMA = 1 - \frac{1}{n}\sum_{j=1}^{n} \alpha_i \left(R_{opt,i} - R_j\right)^2 \tag{15}$$

where α_i is a normalization constant ($\alpha_{CC} = 257.7$ and $\alpha_{CN} = 93.52$) and n is the total number of bonds in the molecule. The optimized bond length, or R_{opt}, is 1.388 Å for a C–C bond and 1.334 Å for a C-N bond. The results of HOMA calculations at the B3LYP/6-31G(d,p) level in the gas and ethanol phases are shown in Table 6. Evidently, Table 6's HOMA results offer a good match with the relative energies and the structure of the thiol-thione tautomer in both gas and ethanol solvent. The strength of HB of thiol in the gas phase can be attributed to the highest value of HOMA (0.89) of the thiophenyl ring. Through the formation of thione tautomer, the five- and six-membered rings exhibit reasonably higher and lower delocalization, with HOMA values of 0.61 and 0.67, respectively. The five-membered ring's lower HOMA values in the thiol form (0.48) compared to the thione (0.61) tautomer indicate that its electron delocalization to the IHB ring in the thiol form is involved. With a slightly higher HOMA value than the five-membered ring due to tautomerization, the seven-membered ring indicates a greater aromatic character. From the HOMA values of all rings, thiol seems to have strong π-stacking ability, hence having more aromaticity and stability in gas phase. In ethanol, the aromaticity of the five- and seven-membered rings of thione is increased (0.66 and 0.76, respectively), which raises the summation of HOMA. Thus, the aromaticity and stability of thione are noticed in ethanol solvent. The comparison of HOMA values for the thiophenyl ring and five-membered ring for R1 in the gas phase (0.92 and 0.44), R2 (0.94 and 0.46) and R3 (0.93 and 0.47) seems to suggest a stronger delocalization and the higher stability of the R2 structure. A slight change observed in ethanol preserves the higher stability of R2 and R3 than R1.

Another aromaticity investigation that can be assessed through magnetic criteria is the NICS[46,47]. That can be defined as the negative value of the absolute magnetic shielding calculated at some selective points. The more negative the NICS values, the more aromatic the ring. The NICS(0) and NICS(1) values are computed at the center and 1A° above the aromatic ring, respectively. Aromatic systems possess negative NICS values, as that indicates the presence of an induced diatropic ring current. Positive NICS values refer to paratropicity and are present in antiaromatic systems. Very small NICS values refer to nonaromatic systems. The NICS indices calculated as a single point at the B3LYP/6–31 G(d,p) level in the gas phase are given in Table 6. According to previous studies of NICS calculation[46,47,77–79], the five-membered ring is more aromatic than the six-membered ring followed by the seven-membered ring. As can be seen from Table 6, the pyrrole ring is more aromatic than benzene, and the aromaticity is less in the seven-membered ring. In the gas phase, the thiophenyl ring of thiol exhibits a larger negative NICS(1)zz value (-18.96 ppm) than thione (NICS(1)zz (-14.57)). In the presence of a polar solvent like ethanol, very minute variations in magnetic indices of aromaticity are seen. Due to the absence of IHB production and an increase in π-electron delocalization, the investigated rotamers exhibit somewhat larger NICS(1)zz values of the thiophenyl ring than thiol.

Compound		Gas-phase		Ethanol	
		$NICS(1)_{zz}$	HOMA	$NICS(1)_{zz}$	HOMA
Thiol	Five-membered ring	− 38.74	0.48	− 38.52	0.54
	Seven-membered ring	− 20.23	0.65	− 20.62	0.69
	Six-membered ring	− 18.96	0.89	− 19.52	0.90
∑ HOMA			2.02		2.13
Thione	Five-membered ring	− 26.27	0.61	− 29.40	0.66
	Seven-membered ring	− 11.63	0.69	− 18.06	0.76
	Six-membered ring	− 14.57	0.67	− 17.29	0.77
∑ HOMA			1.97		2.19
R1	Five-membered ring	− 38.63	0.44	− 38.24	0.49
	Seven-membered ring	− 20.32	0.62	− 20.54	0.66
	Six-membered ring	− 21.83	0.92	− 22.21	0.92
∑ HOMA			1.98		2.07
R2	Five-membered ring	− 34.64	0.46	− 34.09	0.53
	Seven-membered ring	− 19.89	0.64	− 20.17	0.68
	Six-membered ring	− 19.75	0.94	− 19.86	0.93
∑ HOMA			2.04		2.14
R3	Five-membered ring	− 37.60	0.47	− 37.00	0.53
	Seven-membered ring	− 20.85	0.64	− 21.11	0.67
	Six-membered ring	− 22.46	0.93	− 22.58	0.93
∑ HOMA			2.04		2.13

Table 6. The $NICS(1)_{zz}$ (in ppm) and HOMA index of the studied tautomers and rotamers calculated in gas phase and ethanol at the B3LYP/6-31G(d,p). Five- and seven-membered rings of azaazulene and phenyl rings are presented in Fig. 2.

NMR analysis. The high correlation between the experimental[21] and theoretical[22] NMR chemical shifts of 2-(2-hydroxyphenyl)-1-azaazulene (2OHPhAZ) at the B3LYP/6-31G(d,p) level that has been previously recorded[22] imparts trust in the computational techniques utilized. The calculated ^{1}H and ^{13}C NMR chemical shifts δ(ppm) values for the 2-(2-Mercaptophenyl)-1-azaazulene tautomers and rotamers calculated in $CHCl_3$ at the B3LYP/6-31G (d,p) level of theory are listed in Table 7. For the ^{1}H NMR chemical shift, the hydrogen atoms bonded to carbon atoms in aromatic rings, ranging from 6 to 8 ppm[80–82]. The thione NH1 proton and the thiol SH1 proton have high chemical shifts (high downfield shift/low-field proton signal) at δ 18.4 and 13.6 ppm, respectively. While for rotamers, the SH_1 proton was assigned at lower chemical shifts in the range of δ 3.9 to 4.6 ppm. This is due to the presence of HB in the thiol and thione structures and the absence of HB in the structures of rotamers. The azaazulenyl ring and phenyl ring protons in the studied compounds showed a low chemical shift in the range of 7.2 to 8.9 ppm.

The computed ^{13}C NMR chemical shifts for 2-(2-Mercaptophenyl)-1-azaazulene tautomers and rotamers are in the region 104.0–173.8 ppm (in $CHCl_3$). The highest chemical shift values given in thiol are C2 (163.4 ppm) and C2' in thione (173.8 ppm). This low field shift is due to the fact that C2 and C2' are bonded to the high electronegativity N and S atoms and the high polarity of the NH and C = S groups in thiol and thione, respectively. Similarly, C8a has a high chemical shift (greater than 140 ppm) for thiol and all the studied rotamers by connecting to the N atom. The highest chemical shifts of C2' and H1 in the studied thione correlated well with the highest chemical shift of C2' and H1 in the keto of 2OHPhAZ (δ 171.3 and 19.4 ppm, respectivel)[22]. The calculated chemical shift of the thiocarbonyl group (C = S) (173.8 ppm) is in good agreement with the reported

	C2'	H1- S1/N
Thiol	143.35	13.58
Thione	135.12	18.44
R1	127.46	4.02
R2	123.77	4.55
R3	124.22	3.93

Table 7. ^{13}C and ^{1}H NMR chemical shifts (in ppm) calculated for C2' and H1-S/N at the B3LYP/6-31G(d,p) level of theory of 2-(2-Mercaptophenyl)-1-azaazulene tautomer and rotamers using the GIAO method in $CHCl_3$.

chemical shifts of 169.9 and 177.7 ppm for 3-Hydroxy-2-methyl-4-p-pyridinethione[83] and 5-(3-pyridyl)-4H-1,2,4-triazole-3-thione[84], respectively.

UV–Vis spectral analysis. We have found that our previous calculation of 2OHPhAZ[22] using TDDFT-PBE/SMD with a 6–311+G(d,p) basis set level exhibits better quantitative agreement regarding the first and second maximum excitation peaks with the available experimental data[21] than other levels[22]. The calculated UV–vis parameters of the intense peaks in acetonitrile for the studied tautomers and rotamers with the TD-PBE method are presented in Table 8. The calculated UV–vis spectra for all the studied compounds are given in Fig. 4. The thione form is accompanied by a large red shift (extended to 1000 nm), followed by the thiol form (extended to 700 nm), and the lower shift has been found with the rotamers (extended to 600 nm), as depicted in Fig. 4. As can be seen in Table 5, the energy differences between HOMOs and LUMOs are 2.98 eV (for thiol), 1.87 eV (for

Compound	State	E^a	F	Assignment[b]
Thiol	1	2.21(561)	0.1041	H→L (91%)
	5	3.22(385)	0.1554	H-3→L (35%), H-2→L (42%), H-1→L+1 (17%)
	6	3.73(332)	0.3052	H-2→L (11%), H-2→L+1 (17%), H-1→L+1 (50%)
Thione	1	1.58 (783)	0.1103	H→L (94%)
	5	2.72(456)	0.2522	H-2→L (91%)
	9	3.57 (348)	0.2752	H-3→L (38%), H-2→L+1 (38%)
R1	1	2.33 (531)	0.1186	H→L (89%)
	5	3.25 (382)	0.2400	H-2→L (54%), H-1→L+1 (27%), H→L+1 (10%)
	6	3.78 (328)	0.2639	H-2→L+1 (24%), H-1→L+1 (39%), H→L+1 (12%)
	10	4.21 (294)	0.1658	H-4→L (10%), H-1→L+3 (17%), H→L+3 (55%)
R2	1	2.41 (515)	0.1077	H→L (89%)
	4	3.25 (382)	0.2012	H-2→L (41%), H-1→L+1 (19%), H→L+1 (23%)
	6	3.81 (326)	0.1836	H-2→L+1 (37%), H-1→L+1 (32%), H→L+1 (10%)
	8	4.05 (306)	0.1418	H-4→L (11%), H-2→L+1 (27%), H-1→L+1 (10%), H→L+2 (34%)
	10	4.22 (294)	0.1025	H-5→L (14%), H-3→L+1 (27%), H→L+3 (33%)
R3	1	2.45 (506)	0.1034	H-1→L (12%), H→L (81%)
	3	3.13 (396)	0.1283	H-2→L (44%), H→L+1 (45%)
	4	3.22 (385)	0.1138	H-2→L(31%), H-1→L+1 (22%), H→L+1 (35%)
	6	3.78 (328)	0.2062	H-2→L+1 (32%), H-1→L+1 (35%), H→L+1 (12%)
	8	4.11 (301)	0.2557	H-2→L+1 (13%), H→L+2 (64%)

Table 8. Excitation energies (eV) at (TD-PBE-SMD, acetonitrile)/6–311+G(d,p)//B3LYP/6-31G(d,p), oscillator strengths ($f > 0.1$), and their transition characters for 2-(2-Mercaptophenyl)-1-azaazulene tautomers and rotamers. [a]Values in parentheses are given in nm. [b]Only contributions above 10% are shown. H and L represent HOMO and LUMO, respectively.

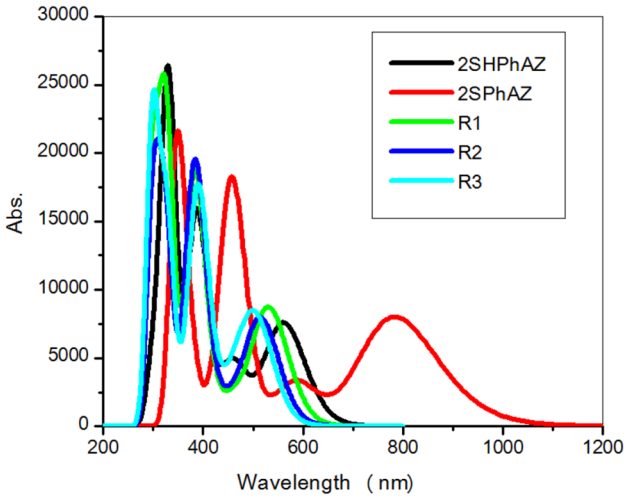

Figure 4. The simulated UV/Vis absorption spectra for the thiol, thione and rotamers of 2-(2-Mercaptophenyl)-1-azaazulene at TD-PBE/6-311+G (d,p).

thione), 3.24 eV (for R1), 2.33 eV (for R2) and 2.23 eV (for R3) in the gas phase. As expected from the lower E_g value of thione, the thione maxima in the electronic absorption spectra are shifted bathochromically by 16, 20, 22 and 47 nm in comparison with thiol, R1, R2, and R3, respectively.

The strong electronic absorption of thione is attributed to the HOMO-3 to LUMO and HOMO-2 to LUMO + 1 transitions. The transitions from to HOMO-2 to LUMO and LUMO + 1 and HOMO-1 to LUMO + 1 cause maximum absorption peak for thiol, which appears at a lower wavelength than thione. However, the strong electronic absorption of the studied rotamers has a different contribution, as shown in Table 8. The NTOs for the high-intensity excited states of the investigated systems are shown in Fig. 5 to analyze the nature of absorption. The occupied and unoccupied NTOs are referred to as "hole" and "particles" transition orbitals, respectively. The NTOs generally give a simpler description of the excited state than the canonical orbitals. As displayed in Fig. 6, where the canonical orbitals were used, the dominant transitions are π-π* for the excitations, with some contribution from n-π* excitation. This makes the analysis of excitations cumbersome. However, as depicted in Fig. 6, the hole NTOs contributing to the illustrated band in Fig. 6 and Table 8 of all studied structures are delocalized over the whole molecular skeleton, while the particle NTOs are mainly delocalized over either azaazulene or benzene rings. This suggests π-π* excitation.

Nonlinear optical (NLO) analysis. It is known that heterocyclic compounds have enhanced charge transfer, which could lead to large nonlinear optical properties. In this section, we will test this information and provide the scientific community any basic information about the hyperpolarizability of these tautomer's and rotamers. Non-linear optical properties (NLO) are the ability of any compound to convert light [with an intense electric field (LASER)] of a longer wavelength into light of a shorter wavelength. One of the non-linear optical phenomena is the second harmonic generation (SHG), where intense light of a longer wavelength is converted to half of the incident value upon absorption by the non-linear optical material.

Most applications of single crystals of any nonlinear material are evident in the fields of semiconductors, infrared detectors, solid state lasers, photosensitive materials, and crystalline thin films for microelectronics[85–87]. The investigation of the relationship between the electronic structure and NLO parameters of the studied compounds is calculated theoretically using ωB97XD/6–311++G(2d,2p) and B3LYP/6–311++g(2d,2p) (Table 9 and S2, respectively). Total static dipole moment (μ), the mean polarizability, the anisotropy of the polarizability Δ, α the mean first-order hyperpolarizability (β), the hyper-Rayleigh scattering (β_{HRS}) and the depolarization ratio (*DR*) of the studied compounds are listed in Table 9. In this study, *P*-nitro aniline (PNA), a standard prototype molecule used in NLO studies, was chosen as a reference as there were no experimental values for the NLO properties of the studied compounds. The values of, $\boldsymbol{\alpha}$ in Table 9 show that the order of increasing $\boldsymbol{\alpha}$ with respect to PNA is: R2, Thiol, and R1 are ~ 3.5 and 3 times higher than PNA, respectively, whereas rotamer R3, and Thione is ~ 4 times higher than the standard PNA at ωB97XD/6–311 + +G(2d,2p). The calculated first order hyperpolarizability β of *p*- nitroacetanilide (PNA) is 15.5×10^{-30} esu as reported by T. Gnanasambandan et al.[88–90] The analysis of the β parameter shows that Thiol, R2, R3, and R1 are ~ 2 times higher than PNA, while rotamer Thione is ~ 2.5 times higher than the reference at ωB97XD/6–311 + +G(2d,2p). Furthermore, for the investigated compound, the lowest value of *DR*, and the highest value of β_{HRS} confirm short bond length, indicating increased selectivity. Therefore, the studies tautomer's and rotamers show promising optical properties.

Conclusions

Five tautomers and rotamers (thiol, thione, R1, R2, and R3) of 2-(2-Mercaptophenyl)-1-azaazulene were studied using density functional theory (DFT). At the B3LYP/6-31G(d,p), the geometrical structural parameters and vibrational frequencies have been discussed. According to the results, B97XD/6–311++G(2d,2p) performs better than CCSD(T)/6–311++G(2d,2p). A very good agreement is seen when compared to the similar molecule 2-(2-hydroxyphenyl)-1-azaazulene. All levels of calculations show that the thiol form is the most stable tautomer in the gas phase. The order of stability is reversed in ethanol as a polar solvent, whereas thione becomes the most stable tautomer. It can be seen that the thione NH1 proton and the thiol SH1 proton have high chemical shifts at δ

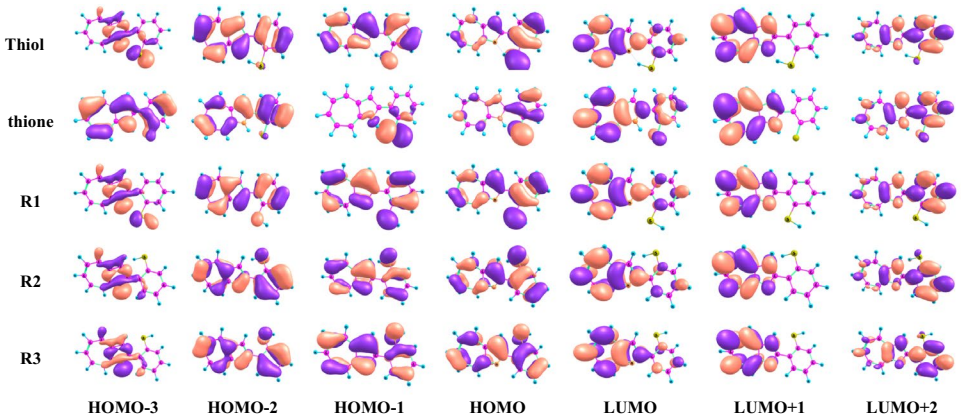

Figure 5. Frontier orbitals of the studied structures at the B3LYP/6-31G(d,p).

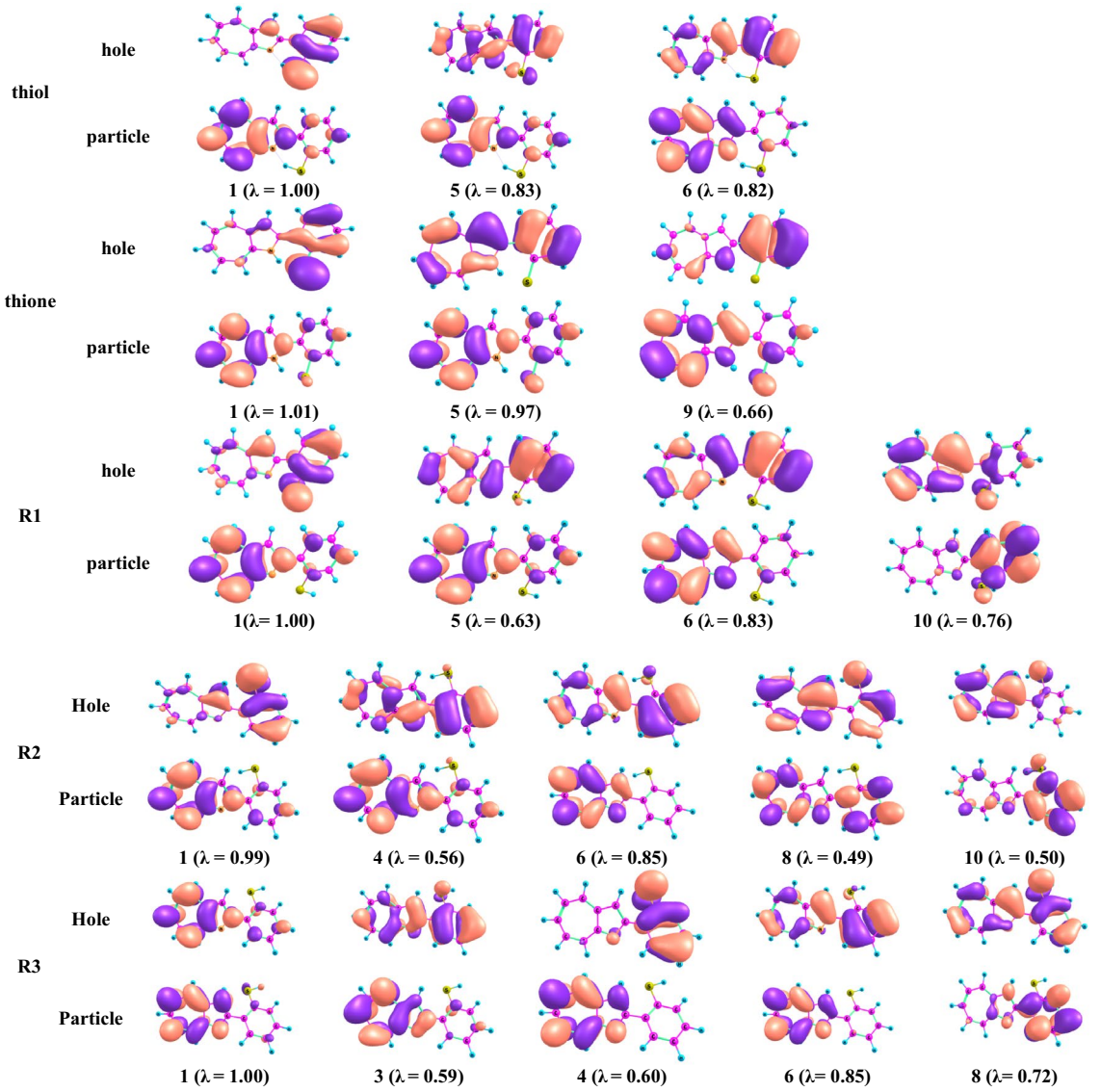

Figure 6. Natural transition orbitals (NTOs) for the excitation with significant and small but non-negligible oscillation strengths for the studied structures at the PBE/6-311+G(d,p) level with solvent effects of acetonitrile through SMD. The displayed occupied (holes) and unoccupied (electrons) NTO pairs are the only that have contributed more than 50% to each excited state (λ is eigenvalues of the pairs).

18.4 and 13.6 ppm, respectively. HOMA and NICS results for aromaticity provide a good match with the relative energies and the structure of the thiol-thione tautomer in both gas and ethanol solvent. The UV–vis absorption spectra of the studied compound have been calculated using the TD-PBE method with a 6–311+G(d,p) basis set for 2-(2-Mercaptophenyl)-1-azaazulene. UV–vis computations indicate that the thione form has a significant red-shift (extended to 1000 nm), followed by the thiol form (extended to 700 nm), and that the rotamers have the lowest red-shift (extended to 600 nm). NTOs are used to indicate the $\pi - \pi^*$ nature of the transitions. In comparison to the PNA molecule, the studied molecules offer good benefits in technology-related applications. According to the NLO study, tautomers and rotamers show promising optical properties.

Property	PNA	Thiol	Thione	R1	R2	R3
μ_x, D		−4.1	−8.0	−2.1	3.2	1.7
μ_y, D		−2.5	−4.2	−1.6	0.4	0.9
μ_z, D		0.0	0.0	0.2	−0.6	−0.5
μ, Debye[a]	2.4	4.8	9.0	2.7	3.3	2.0
α_{XX}, a.u		−81.0	−83.2	−77.2	−81.2	−75.2
α_{XY}, a.u		−5.7	−11.0	−0.1	4.6	−0.7
α_{YY}, a.u		−98	−103.4	−94.7	−100.3	−97.5
α_{ZZ}, a.u		−113.8	−114.1	−113.6	−111.2	−112.8
α_{YZ}, a.u		1.3	0.0	−0.4	−1.2	−1.1
α_{XZ}, a.u		0.5	0.0	0.3	1.6	−0.3
$<\alpha> \times 10^{-24}$ esu[b]	22	30.1	33.3	31.5	27.7	32.8
$\Delta\alpha \times 10^{-24}$ esu		97.6	100.2	95.2	97.6	95.16
βxxx, a.u		−58.9	−102.7	−32.9	56.6	28.8
βxxy, a.u		−11.4	−24.3	9.5	−19.2	5.4
βxyy, a.u		−27.5	−52.5	−5.1	17.1	0.1
βyyy, a.u		−18.7	−39.9	−4.2	−8.3	2.6
βxxz, a.u		−0.7	0.0	2.2	−4.9	6.2
βxyz, a.u		−7.4	0.0	10.2	−14.6	−17.2
βyyz, a.u		0.9	0.0	2.5	−3.9	−1.9
βxzz, a.u		−2.2	−4.4	−0.8	4.5	2.5
βyzz, a.u		1.8	1.1	2.8	3.9	1.8
βzzz, a.u		0.4	0.0	−0.1	2.9	1.6
$<\beta^{>} \times 10^{-30}$ esu[c]	15.5	61.8	110.2	33.2	57.2	28.9
DR		0.3	0.0	2.8×10^{-3}	0.4	0.1
β_{HRS}		0.7	6×10^{-4}	2.2	5.7	6.4

Table 9. Total static dipole moment (μ), the mean polarizability ($<\alpha>$), the anisotropy of the polarizability ($\Delta\alpha$), and the mean first-order hyperpolarizability ($<\beta>$), for the studied compounds (Thiol, Thione, R1, R2, and R3) computed at ωB97XD/6–311++G(2d,2p). [a,b,c]PNA results are taken from ref[88–90].

Data availability

All data used or analysed during the current study are included in this published article [and its supplementary information files.

Received: 6 June 2023; Accepted: 10 September 2023
Published online: 20 September 2023

References

1. Abood, N. A. & Al-Shlhai, R. A. Theoretical study of molecular structure, IR and NMR spectra of pyrazolone and its derivatives. *J. Chem. Pharm. Res.* **4**(3), 1772–1781 (2012).
2. Sugavara, T. & Takasu, I. Tautomerism in the Solid State. *Adv. Phys. Org. Chem.* **32**, 219–265 (1999).
3. Willner, I., Rubin, S. Angew. Control of the structure and functions of biomaterials by light. *Chem. Int. Ed. Engl.* **35,** 367–385 (1996).
4. Sytnik, A. & Del Vale, J. C. Steady-state and time-resolved study of the proton-transfer fluorescence of 4-hydroxy-5-azaphenanthrene in model solvents and in complexes with human serum. *J. Phys. Chem.* **99**, 13028–13032 (1995).
5. Guha, D. *et al.* Proton transfer reaction of a new orthohydroxy Schiff base in protic solvents at room temperature. *Spectrochim. Acta Part A Mol. Biomol. Spectrosc.* **56**(14), 2669–2677 (2000).
6. Zgierski, M. & Grabowska, A. Theoretical approach to photochromism of aromatic Schiff bases: A minimal chromophore salicylidene methylamine. *J. Chem. Phys.* **113**, 7845–7852 (2000).
7. Elguero, J., Marzin, C., Katritzky, A. R., Linda, P. The Tautomerism of Heterocycles, New York, (1976).
8. Nowak, M. J., Lapinski, L., Rostkowska, H., Les´, A., Adamowicz, L. Theoretical and matrix-isolation experimental study on 2 (1H)-pyridinethione/2-pyridinethiol. *J. Phys.Chem.* **94,** 7406–7414 (1990).
9. tautomerism and phototautomerism. Nowak, M. J., Lapinski, L., Fulara, J., Les´ A., Adamowicz, L. Theoretical and infrared matrix isolation study of 4 (3H)-pyrimidinethione and 3 (2H)-pyridazinethione. *J. Phys. Chem.* **95**, 2404–2411 (1991).
10. Prusinowska, D., Lapinski, L., Nowak, M. J. & Adamowicz, L. Tautomerism, phototautomerism and infrared spectra of matrix-isolated 2-quinolinethione. *Spectrochim. Acta, Part A* **51**, 1809–1826 (1995).
11. Bràs, E. M. & Fausto, R. An insight into methimazole phototautomerism: Central role of the thiyl radical and effect of benzo substitution. *J. Mol. Struct.* **1172**, 42–54 (2018).
12. Bràs, E. M. & Fausto, R. Controlled light-driven switching in 2-thiobenzimidazole. *J. Photochem. Photobiol. A.* **357**, 185–192 (2018).
13. Rostkowska, H., Lapinski, L., Khvorostov, A. & Nowak, M. J. Proton-transfer processes in thiourea: UV induced thione→ thiol reaction and ground state thiol→ thione tunneling. *J. Phys. Chem. A* **107**, 6373–6380 (2003).
14. Lapinski, L., Rostkowska, H., Khvorostov, A. & Nowak, M. J. UV induced proton transfer in thioacetamide: first observation of thiol form of simple thioamide. *Phys. Chem. Chem. Phys.* **5**, 1524–1529 (2003).
15. Reva, I., Nowak, M. J., Lapinski, L. & Fausto, R. Hydrogen atom transfer reactions in thiophenol: photogeneration of two new thione isomers. *Phys. Chem. Chem. Phys.* **17**, 4888–4898 (2015).

16. Metzner, P. *Organic Compounds of Sulphur, Selenium, and Tellurium* (Chem. Soc, 1979).
17. Block, E. *Reactions of Organosulfur Compounds: Organic Chemistry: A Series of Monographs.* **37,** Academic press. (2013).
18. Maw, G. A. "Sulfur in Organic and Inorganic Chemistry (Senning, A., Ed.)." (1972).
19. Steliou, K., & Mrani, M. Reagents for organic synthesis. Tin-assisted sulfuration: a highly potent new method for the conversion of carbonyl units into their corresponding thiocarbonyl analogs. *J. Am. Chem. Soc.* **104**, 3104–3106 (1982).
20. Abe, N. & Gunji, T. The Chemistry of Azaazulenes. *Heterocycles* **82**, 201–248 (2010).
21. Oda, M. Synthesis, Molecular Structure, and Properties of 2-(2-Hydroxyphenyl)-1-azaazulene. *J. Org. Chem.* **6**, 2231–2236 (2012).
22. El-Meligy, A. B.*et. al.* Structures, Energetics, and Spectra of (NH) and (OH) Tautomers of 2-(2-Hydroxyphenyl)-1-azaazulene: A Density Functional Theory/Time-Dependent Density. *ACS Omega*. **7**, 14222–14238 (2022).
23. Tuncel, D. π-Conjugated nanostructures materials: preparation, properties, and Photonic applications. *Nanoscale Advances* **1**, 19–33 (2019).
24. Davari, M. D., Bahrami, H., Haghighi, Z. Z. & Zahed, M. Quantum chemical investigation of intramolecular thione-thiol tautomerism of 1,2,4-triazole-3-thione and its disubstituted derivatives. *J. Mol. Model.* **16**, 841–855 (2010).
25. Özdemir, N. Quantum chemical investigation of the intra-and intermolecular proton transfer reactions and hydrogen bonding interactions in 4-amino-5-(2-hydroxyphenyl)-2H-1, 2,4-triazole-3(4H)-thione. *J. Mol. Model* **19**(1), 397–406 (2013).
26. Sheikhshoaie, I. & Fabian, W. M. F. Theoretical insights into material properties of Schiff bases and related azo compounds. *Curr Org Chem.* **13**, 149–171 (2009).
27. Nemykin, V. N., Olsen, J. G., Perera, E. & Basu, P. Synthesis, Molecular and Electronic Structure, and TDDFT and TDDFT-PCM Study of the Solvatochromic Properties of (Me_2Pipdt) Mo $(CO)_4$ Complex (Me_2Pipdt= N. *Inorg. Chem.* **45**, 3557–3568 (2006).
28. Greenwood, J. R., Calkins, D., Sullivan, A. P. & Shelley, J. C. Towards the comprehensive, rapid, and accurate prediction of the favorable tautomeric states of drug-like molecules in aqueous solution. *J Comput Aided Mol Des.* **24**, 591–604 (2010).
29. Lamsabhi, M. Specific Hydration Effects on Oxo–Thio Triazepine Derivatives. *J. Phys. Chem. A* **112**, 1791–1797 (2008).
30. Becke, A. D. A new mixing of Hartree-Fock and local density-functional theories. *J. Chem. Phys.* **98**, 1372–1376 (1993).
31. Lee, C., Yang, W. & Parr, R. G. Development of the Colle-Salvetti correlation-energy formula into a functional of the electron density. *Phys. Rev. B Condens. Matter.* **37**, 785–789 (1988).
32. Rassolov, V. A., Ratner, M. A., Pople, J. A., Redfern, P. C. & Curtiss, L. A. *J. Comput. Chem.* **22**, 976–984 (2001).
33. Frisch, M. J., Trucks, G. W., Schlegel, H. B., Scuseria, G. E.. *et al.*, Gaussian, Inc., Wallingford CT, Version 9.0 (2009).
34. GaussView, V. *5, R* (T. Keith, J. Millam, Semichem Inc., Shawnee Mission KS, 2009).
35. http://www.chemcraftprog.com.
36. Zhao, Y. & Truhlar, D. G. The M06 Suite of Density Functionals for Main Group Thermochemistry, Thermochemical Kinetics, Noncovalent Interactions, Excited States, and Transition Elements: Two New Functionals and Systematic Testing of Four M06 Class Functionals and 12 Other Function. *Theor. Chem. Acc.* **120**, 215–241 (2008).
37. Chai, J. D. & Head-Gordon, M. Systematic Optimization of Long-Range Corrected Hybrid Density Functionals. *J. Chem. Phys.* **128**, 084106–084114 (2008).
38. Mardirossian, N., Head-Gordon, M. ωB97XD: A 10Parameter, Range-Separated Hybrid, Generalized Gradient Approximation Density Functional with Nonlocal Correlation. Designed by a Survival-of-the-Fittest Strategy. *Phys. Chem. Chem. Phys.* **16,** 9904–9924 (2014).
39. Lin, Y. S., Li, G.-D., Mao, S. P. & Chai, J. D. Long-Range Corrected Hybrid Density Functionals with Improved Dispersion Corrections. *J. Chem. Theory Comput.* **9**, 263–272 (2013).
40. Purvis, G. D. & Bartlett, R. J. A Full Coupled-Cluster Singles and Doubles Model: The Inclusion of Disconnected Triples. *J. Chem. Phys.* **76**, 1910–1918 (1982).
41. Marenich, A. V., Cramer, C. J. & Truhlar, D. G. Universal Solvation Model Based on Solute Electron Density and on a Continuum Model of the Solvent Defined by the Bulk Dielectric Constant and Atomic Surface Tensions. *J. Phys. Chem. B.* **113**, 6378–6396 (2009).
42. Hill, T. L. *Introduction to Statistic Thermodynamics* (Addison-Wesley, 1960).
43. Canneaux, S., Bohr, F. & Henon, E. KiSThelP: A Program to Predict Thermodynamic Properties and Rate Constants from Quantum Chemistry Results. *J. Comput. Chem.* **35**, 82–93 (2014).
44. Wigner, E. On the quantum correction for thermodynamic equilibrium. *Phys. Rev.* **40**, 203 (1932).
45. Mishra, V. R. & Sekar, N. Photostability of Coumarin Laser Dyes - a Mechanistic Study Using Global and Local Reactivity Descriptors. *J. Fluoresc.* **27**, 1101–1108 (2017).
46. Schleyer, P. V. R., Maerker, C., Dransfeld, A., Jiao, H. & van Eikema Hommes, N. J. Nucleus-Independent Chemical Shifts: A Simple and Efficient Aromaticity Probe. *J. Am. Chem. Soc.* **118**, 6317–6318 (1996).
47. Stanger, A. Nucleus-Independent Chemical Shifts (NICS): Distance Dependence and Revised Criteria for Aromaticity and Antiaromaticity. *J. Org. Chem.* **71**, 883–893 (2006).
48. Krygowski, T. M. Crystallographic Studies of Inter- and Intermolecular Interactions Reflected in Aromatic Character of Pi- Electron Systems. *J. Chem. Inf. Comput. Sci.* **33**, 70–78 (1993).
49. Kruszewski, J. & Krygows, T. M. Definition of Aromaticity Basing on the Harmonic Oscillator Model. *Tetrahedron Lett.* **13**, 3839–3842 (1972).
50. Perdew, J. P., Burke, K. & Ernzerhof, M. Generalized Gradient Approximation Made Simple. *Phys. Rev. Lett.* **77**, 3865–3868 (1996).
51. Ernzerhof, M. & Perdew, J. P. Generalized Gradient Approximation to the Angleand System Averaged Exchange Hole. *J. Chem. Phys.* **109**, 3313–3320 (1998).
52. O'Boyle, N. M., Tenderholt, A. L. & Langner, K. M. Cclib: A Library for Package-Independent Computational Chemistry Algorithms. *J. Comput. Chem.* **29**, 839–845 (2008).
53. Martin, R. L. Natural Transition Orbitals. *J. Chem. Phys.* **118**, 4775–4777 (2003).
54. Wolinski, K., Hinton, J. F. & Pulay, P. Efficient Implementation of the Gauge-Independent Atomic Orbital Method for NMR Chemical Shift Calculations. *J. Am. Chem. Soc.* **112**, 8251–8260 (1990).
55. Wolff, S. K. & Ziegler, T. Calculation of DFT-GIAO NMR Shifts with the Inclusion of Spin-Orbit Coupling. *J. Chem. Phys.* **109**, 895–905 (1998).
56. Szafran, M., Komasa, A. & Bartoszak-Adamska, E. Crystal, and molecular structure of 4-carboxypiperidinium chloride (4-piperidinecarboxylic acid hydrochloride). *J. Mol. Struct.* **827**, 101–107 (2007).
57. Avci, D. Second and third-order nonlinear optical properties and molecular parameters of azo chromophores: semiempirical analysis. *Spectrochim. Acta A.* **82**, 37–43 (2011).
58. Tomasz, S., Katarzyna, S. & Benoît, C. Ab initio Hartree-Fock calculations on linear and second-order nonlinear optical properties of ionic organic crystals. *J. Chem. Phys.* **141**, 104109 (2014).
59. Walker, M., Harvey, A. J. A., Sen, A. & Dessent, C. E. H. Performance of M06, M06–2X, and M06-HF Density Functionals for Conformationally Flexible Anionic Clusters: M06 Functionals Perform Better than B3LYP for a Model System with Dispersion and Ionic Hydrogen-Bonding Interactions. *J. Phys. Chem. A.* **117**, 12590–12600 (2013).
60. Kaczorowska, M. A., Kaczmarek-Kędziera, A., Só miałowski, B. Tautomeric Equilibrium, Proton Affinity and Mass Spectrometry Fragmentation of Flexible Hydrogen-Bonded Precursors and Rigid N → BF_2 Fluorescent Dyes. *Sci. Rep.* **11,** 87–100 (2021).
61. Berenbeim, J. A. *et al.* Unravelling the Keto–Enol Tautomer Dependent Photochemistry and Degradation Path- ways of the Protonated UVA Filter Avobenzone. *J. Phys. Chem. A* **124**, 2919–2930 (2020).

62. Gad, S. F., El-Demerdash, S. H., El-Mehasseb, I. M. & El-Nahas, A. M. Structure, Stability and Conversions of Tautomers and Rotamers of Azulene-Based Uracil Analogue. *J. Mol. Struct.* **118**(2), 271–282 (2019).
63. Mezey, P. G. & Ladik, J. J. A non-empirical molecular orbital study on the relative stabilities of adenine and guanine tautomers. *Theor Chim Acta.* **52**, 129–145 (1979).
64. Mezey, P. G., Ladik, J. J. & Barry, M. Non-empirical SCF MO studies on the protonation of biopolymer constituents. *Theor Chim Acta.* **54**, 251–258 (1979).
65. Turecek, F. Proton Affinity of Dimethyl Sulfoxide and Relative Stabilities of C_2H_6OS Molecules and $C_2H_7OS^+$ Ions. A Comparative G2(MP2) ab Initio and Density Functional. *J. Phys. Chem. A.* **102,** 4703–4713 (1998).
66. Frank, A. J., Sadilek, M., Ferrier, J. G. & Turecek, F. Hydroxysulfinyl radical and sulfinic acid are stable species in the gas phase. *J. Am. Chem Soc.* **118**, 11321–11322 (1996).
67. old problems-new answers. Beak, P. Acc. Energies and alkylations of tautomeric heterocyclic compounds. *Chem. Res.* **10**, 186–192 (1977).
68. Katritzky, A. R., Jug, K. & Oniciu, D. C. Quantitative Measures of Aromaticity for Mono-, Bi-, and Tricyclic Penta- and Hexaatomic Heteroaromatic Ring Systems and Their Interrelationships. *Chem. Rev.* **101**(5), 1421–1450 (2001).
69. Stoyanov, S., Stoyanova, T., Akrivos, P. D., Karagiannidis, P. & Nikolov, P. Spectroscopic and computational investigation of the ground and low excited states of some symmetrical heterocyclic disulfides. *J. Heterocycl. Chem.* **33**, 927–931 (1996).
70. Beak, P., Covington, J. B. & White, J. M. Quantitative model of solvent effects on hydroxypyridine-pyridone and mercaptopyridine-thiopyridone equilibriums: correlation with reaction-field and hydrogen-bonding effects. *J. Org. Chem.* **45**, 1347–1353 (1980).
71. Woodward, R. B. & Hoffmann, R. *The Conservation of Orbital Symmetry* (Chemie, 1970).
72. Uesugi, Y., Mizuno, M., Shimojima. A., Takahashi, H. Transient Resonance Raman and Ab-Initio Mo Calculation Studies of the Structures and Vibrational Assignments of the t1 State and the Anion Radical of Coumarin and Its Isotopically Substituted Analogues. *J. Phys. Chem.* **101,** 268–274 (1997).
73. Sinha, L., Prasad, O., Narayan, V., Shukla, S. & Raman, R. FT-IR Spectroscopic Analysis and First-Order Hyperpolarisability of 3-benzoyl-5-chlorouracil by First Principles. *Mol. Simul.* **37**, 153–163 (2011).
74. Pearson, R. G. Hard and Soft Acids and Bases. *J. Am. Chem. Soc.* **85**, 3533–3539 (1963).
75. Grabowski, S. J., Leszczynski, J. Unrevealing the nature of hydrogen bonds: π-electron delocalization shapes H-bond features, in: J. Slawomir (Ed.). Hydrogen Bonding–New Insights. Grabowski Kluwer, (2006).
76. Domingo, L. R. Molecular electron density theory: a modern view of reactivity in organic chemistry. *Molecules* **21**(10), 1319 (2016).
77. Dominikowska, J. Palusiak, M. EL. the New Aromaticity Measure Based on One-Electron Density Function. *Struct. Chem.* **23,** 1173–1183 (2012).
78. Frizzo, C. P. & Martins, M. A. P. Aromaticity in Heterocycles: New HOMA Index Parametrization. *Struct. Chem.* **23**, 375–380 (2012).
79. Corminboeuf, C., Heine, T. & Webera, J. Evaluation of Aromaticity: A New Dissected NICS Model Based on Canonical Orbitals. *Phys. Chem. Chem. Phys.* **5**, 246–251 (2003).
80. Anderson, R. J. & Bendell, P. W. *Groundwater* (Organic Spectroscopic Analysis. The Royal Society of Chemistry, 2004).
81. Kalinowski, H. O., Berger, S. & Braun, S. *Carbon-13 NMR Spectroscopy* (John Wiley & Sons, 1988).
82. Pihlaja, K. K. & E., (eds) *Carbon-13 Chemical Shifts in Structural and Sterochemical Analysis* (VCH Publishers, 1994).
83. Monga, V., O.Patrick, B., Orvig, C. Group 13 and Lanthanide Complexes with Mixed *O*, *S* Anionic Ligands Derived from Maltol. *Inorg. Chem.* **44,** 2666–2677 (2005).
84. Gökce, H., Öztürk, N., Ceylan, Ü., Bingöl, Y. & Alpaslan, G. Alpaslan, tautomeric analysis, spectroscopic (FT-IR, Laser-Raman, NMR and UV–vis) properties and DFT computations of 5-(3-pyridyl)-4H-1, 2, 4-triazole-3-thiol molecule. *Spectrochim. Acta Part A Mol. Biomol. Spectrosc.* **163**, 170–180 (2016).
85. Chemia, D. S., Zysss, J. Nonlinear Optical Properties of Organic Molecules and Crystals *New York* 19872 (1987).
86. Bradshow, D. S. & Andrews, D. L. Quantum Channels in Nonlinear Optical process. *J. Nonlinear Opt Phys. Matter.* **18**, 285–299 (2009).
87. Sures, S. The Growth and the Optical, Mechanical, Dielectric and Photoconductivity Properties of a New Nonlinear Optical Crystal—L-Phenylalanine-4-nitrophenol NLO Single Crystal Scientific-Research an Academic Publisher1. **3,** 87–91 (2013).
88. Cheng, L. T. *et al.* Electric field induced second harmonic generation with and without fringes. *J. Phys. Chem.* **95**, 10631–10640 (1991).
89. Kaatz, P., Donley, E. A. & Shelton, D. P. Analysis of nonlinear optical properties in donor–acceptor materials. *J. Chem. Phys.* **108**, 849–858 (1998).
90. Gnanasambandan, T., Gunasekaran, S., Seshadri, S. Experimental and theoretical study of *p*-nitroacetanilide. *Spectrochimica. Acta Part A: Molecular and Biomolecular Spectroscopy.* **117**, 557–567 (2014).

Author contributions

A.E.-M performed the calculations. S.E.-D. and A.E.-M collected the data and draw the first version of the manuscript. S.A. checked the paper and prepared Table 8 and Fig. 6. A.E.-N. Supervision & review. A.E.-M and A.E.-D. edit & review and improved the paper to be in the final form.

Funding

Open access funding provided by The Science, Technology & Innovation Funding Authority (STDF) in cooperation with The Egyptian Knowledge Bank (EKB).

Competing interests

The authors declare no competing interests.

Additional information

Supplementary Information The online version contains supplementary material available at https://doi.org/10.1038/s41598-023-42450-1.

Correspondence and requests for materials should be addressed to S.H.E.-D. or A.B.E.-M.

Reprints and permissions information is available at www.nature.com/reprints.

Publisher's note Springer Nature remains neutral with regard to jurisdictional claims in published maps and institutional affiliations.